Monopole clustering and color confinement in the multi-instanton system

M. Fukushima,* H. Suganuma, and H. Toki
Research Center for Nuclear Physics, Osaka University, 10-1 Mihogaoka, Ibaraki, Osaka, 567-0047, Japan
(Received 5 February 1999; published 27 September 1999)

We study color confinement properties of the multi-instanton system, which seems to carry an essence of the nonperturbative QCD vacuum. Here we assume that the multi-instanton system is characterized by the infrared suppression of instantons as $f(\rho)\sim\rho^{-5}$ for large size ρ. We first investigate a monopole clustering appearing in the maximally Abelian (MA) gauge by considering the correspondence between instantons and monopoles. In order to clarify the infrared monopole properties, we make the ''block-spin'' transformation for monopole currents. The feature of monopole trajectories changes drastically with the instanton density. At a high instanton density, there appears one very long and highly complicated monopole loop covering the entire physical vacuum. Such a global network of long-monopole loops resembles the lattice QCD result in the MA gauge. Second, we observe that the SU(2) Wilson loop obeys an area law and the static quark potential is approximately proportional to the distance R between quark and antiquark in the multi-instanton system using the SU(2) lattice with a total volume of $V=(10\,\mathrm{fm})^4$ and a lattice spacing of $a=0.05$ fm. We extract the string tension from the 5×10^6 measurements of Wilson loops. With an instanton density of $(N/V)=(1/\mathrm{fm})^4$ and an average instanton size of $\bar{\rho}=0.4$ fm, the multi-instanton system provides a string tension of about 0.4 GeV/fm. [S0556-2821(99)05317-5]

PACS number(s): 11.15.Ha, 12.38.Aw

I. INTRODUCTION

Quantum chromodynamics (QCD) has been established as the fundamental theory of the strong interaction. In the infrared region, there appear various nonperturbative phenomena such as color confinement and dynamical chiral-symmetry breaking. Since the QCD vacuum is composed of gluon fields interacting in a highly complicated way, it is hard to understand these phenomena from perturbative points of view. On the other hand, a topological aspect may provide a useful approach for descriptions of the QCD vacuum. Actually, there appear two nontrivial topological objects, *instantons* and *monopoles*, due to the nonlinearity of QCD.

The instanton configuration discovered in 1975 by Belavin, Polyakov, Shvarts and Tyupkin [1] is a classical and self-dual solution of the Euclidean field equation in Yang-Mills theory. The appearance of instantons corresponds to a homotopy group, $\Pi_3(\mathrm{SU}(N_c))=\mathrm{Z}_\infty$ [2]. Instantons are important for nonperturbative phenomena related to the $\mathrm{U_A}(1)$ anomaly and the large η' mass [3]. Chiral-symmetry breaking could also be interpreted as the instanton effect [4–6]. However, until now there has been no evidence that instantons have anything to do with color confinement in 4-dimensional gauge theory, although Polyakov discovered that instantons cause confinement in certain 3-dimensional Georgi-Glashow models [7]. With recent computational progress, instanton properties are investigated by lattice QCD simulations based on the cooling procedures, which are achieved by an artificial reduction of the local lattice action. This method allows one to eliminate short-range quantum fluctuations of gluon fields and to extract only topological excitations like instantons from the nonperturbative QCD vacuum [8–13]. These investigations provide us the average instanton size $\bar{\rho}\simeq(0.33-0.4)$ fm and the instanton number density $(N/V)\simeq1$ fm^{-4} [8–14]. Although the existence of instantons with high density is agreed upon, the detailed numbers for $\bar{\rho}$ and the size distribution depend largely on the cooling procedure. These scale parameters suggest that the QCD vacuum is the dense matter of instantons and anti-instantons.

In 1981, 't Hooft proposed the Abelian gauge, where the color-magnetic monopole appears as a relevant degree of freedom for the description of color confinement [15]. In the Abelian gauge, the SU(N_c) non-Abelian gauge theory is reduced to the $\mathrm{U}(1)^{N_c-1}$ Abelian gauge theory with color-magnetic monopoles. The appearance of magnetic monopoles corresponds to another homotopy group, $\Pi_2(\mathrm{SU}(N_c)/\mathrm{U}(1)^{N_c-1})=\mathrm{Z}_\infty^{N_c-1}$, which is different from that of instantons. In the Abelian gauge the color confinement mechanism can be interpreted as the dual Meissner effect due to monopole condensation, which is a dual version of Cooper pair condensation in the ordinary superconductivity. Such a dual superconductor picture for color confinement was proposed by Nambu, 't Hooft and Mandelstam in the middle of the 1970's [16–18]. By lattice QCD simulations, it is observed that large monopole clustering covers the entire physical vacuum in the confinement phase, which is identified as a signal of monopole condensation being responsible for confinement [19,20]. Many studies indicate that the monopole is a relevant degree of freedom for color confinement and chiral-symmetry breaking [21–28].

Recent studies show remarkable facts that instantons are directly related to monopoles [29–47] in the Abelian gauge, although these topological objects belong to different homotopy group. For example, in the Polyakov-like gauge [29], monopoles appear due to the existence of the hedgehog configurations near instanton centers. Such correlations indicate that instantons may be important for the promotion of long

*Email address: masa@rcnp.osaka-u.ac.jp

monopole loops. Therefore, we take the multi-instanton system instead of the QCD vacuum in order to clarify monopole clustering and confinement properties in terms of instantons.

II. TOPOLOGICAL OBJECTS IN THE QCD VACUUM

The instanton is a classical and nontrivial solution of the Euclidean Yang-Mills theory, whose action is written as $S=\int d^4x G^a_{\mu\nu}G^a_{\mu\nu}/4g^2$. Here, in order to make the notation and the discussion simpler, we take the SU(2) case and represent $A_\mu(x)\equiv igA^a_\mu(x)\tau^a/2$ and $G_{\mu\nu}(x)\equiv igG^a_{\mu\nu}(x)\tau^a/2$, which are defined as the anti-Hermite variables. Instanton and anti-instanton configurations are characterized by the (anti-)self-duality condition,

$$G^a_{\mu\nu}=\pm\tilde{G}^a_{\mu\nu}, \tag{1}$$

by using the dual field strength $\tilde{G}_{\mu\nu}\equiv\frac{1}{2}\varepsilon_{\mu\nu\alpha\beta}G_{\alpha\beta}$. This condition provides the minimal action $S=(8\pi^2/g^2)|\mathcal{Q}|$. Here, the topological charge is defined as $\mathcal{Q}\equiv\int d^4x\{G^a_{\mu\nu}\tilde{G}^a_{\mu\nu}\}/32\pi^2$. These instanton solutions satisfy the general Yang-Mills field equations automatically, $D_\mu G_{\mu\nu}=\pm D_\mu\tilde{G}_{\mu\nu}=0$. The self-dual solution with $\mathcal{Q}=1$ in the singular gauge [2] is written as

$$A^I_\mu(x;z,\rho,O)=\frac{\tau^a}{2}\frac{2iO^{ab}\bar{\eta}^{b\mu\nu}(x-z)_\nu\rho^2}{(x-z)^2\{(x-z)^2+\rho^2\}}. \tag{2}$$

Here, the instanton solutions have several collective modes related to the size ρ and the position z of instanton, which are described by one and four parameters, respectively. For pure SU(2) gauge theory, the instanton solution can be rotated in color space by the color orientation matrix O, which is characterized by 3 parameters as the Euler angle. The 't Hooft symbol $\bar{\eta}^{b\mu\nu}$ is defined as

$$\bar{\eta}^{b\mu\nu}=-\bar{\eta}^{b\nu\mu}\equiv\begin{cases}\varepsilon^{b\mu\nu}, & \mu,\nu=1,2,3,\\ -\delta^{b\mu}, & \nu=4.\end{cases} \tag{3}$$

The anti-self-dual solution $\bar{A^I_\mu}$ is obtained by replacing $\bar{\eta}^{b\mu\nu}$ to $\eta^{b\mu\nu}\equiv(-1)^{\delta^{\mu4}+\delta^{\nu4}}\bar{\eta}^{b\mu\nu}$ in Eq. (2).

Now, let us discuss the appearance of QCD-monopoles in the Abelian gauge. We consider the maximally Abelian (MA) gauge [19], which is defined in the Euclidean SU(2) QCD by minimizing the variable

$$R_{ch}[A_\mu]=\int d^4x\{(A^1_\mu(x))^2+(A^2_\mu(x))^2\} \tag{4}$$

under the gauge transformation $\Omega(x)$. In the MA gauge, the off-diagonal fields are suppressed by the gauge transformation and the full gauge field $A_\mu=A^a_\mu(\tau^a/2)$ behaves as the abelian gauge field $a_\mu=A^3_\mu(\tau^3/2)$ approximately. In this paper, we adopt the MA gauge, where the Abelian dominance holds for the nonperturbative QCD phenomena [22]. Under the gauge transformation, the gauge field transforms as

$$A_\mu(x)\to A^\Omega_\mu(x)=\Omega(x)(A_\mu(x)+\partial_\mu)\Omega(x)^\dagger. \tag{5}$$

After the gauge fixing, there only remains the Abelian gauge symmetry $U(1)^{N_c-1}\subset SU(N_c)$. When we meet hedgehog configurations like instantons, the multivaluedness happens to the gauge function $\Omega(x)$ and the gauge transformation of Eq. (5) develops a singularity. This singularity leads to the monopole current k_μ. The field strength is defined generally as $G_{\mu\nu}\equiv[\hat{D}_\mu,\hat{D}_\nu]-[\hat{\partial}_\mu,\hat{\partial}_\nu]$ [48], which returns to the standard definition $G_{\mu\nu}=[\hat{D}_\mu,\hat{D}_\nu]=\partial_\mu A_\nu-\partial_\nu A_\mu+[A_\mu,A_\nu]$ for the regular case. Under the singular gauge transformation $\Omega(x)$, the field strength transforms as

$$G^\Omega_{\mu\nu}=\Omega G_{\mu\nu}\Omega^\dagger=\partial_\mu A^\Omega_\nu-\partial_\nu A^\Omega_\mu+[A^\Omega_\mu,A^\Omega_\nu]-\Omega[\partial_\mu,\partial_\nu]\Omega^\dagger. \tag{6}$$

Since the last term is diagonal, Abelian field strength is naturally obtained as

$$F_{\mu\nu}=\partial_\mu a_\nu-\partial_\nu a_\mu-\Omega[\partial_\mu,\partial_\nu]\Omega^\dagger, \tag{7}$$

by performing the Abelian projection, $A^\Omega_\mu\overset{AP}{\to}a_\mu\equiv\mathrm{tr}(A^\Omega_\mu\tau^3)(\tau^3/2)$. The Abelian Bianchi identity is broken due to the existence of the last term in Eq. (7), and the magnetic current $k_\mu(x)$ is obtained as

$$k^\mu(x)\equiv\frac{1}{2}\varepsilon_{\mu\nu\alpha\beta}\partial_\nu F_{\alpha\beta}=-\frac{1}{2}\varepsilon_{\mu\nu\alpha\beta}\partial_\nu\Omega[\partial_\alpha,\partial_\beta]\Omega^\dagger. \tag{8}$$

The obvious consequence of the monopole current conservation, $\partial_\mu k^\mu=0$, means that monopole currents form closed loops.

III. CORRELATION BETWEEN INSTANTON AND MONOPOLE FOR COLOR CONFINEMENT

Recently, both analytical and lattice studies showed a strong correlation between instantons and monopoles in the Abelian projected theory of QCD [29–47]. Let us briefly review recent studies on the correlation between these topological objects in the MA gauge [35,39]. The minimizing condition of $R_{ch}[A_\mu]$ in Eq. (4) satisfies the local condition,

$$(\partial_\mu\mp A^3_\mu)A^\pm_\mu=0,\quad A^\pm_\mu\equiv A^1_\mu\pm iA^2_\mu. \tag{9}$$

It is noted that self-dual solutions such as an instanton satisfy the stationary condition (9) automatically. However, this stationary condition is not sufficient to realize the MA gauge. In the MA gauge the functional $R_{ch}[A_\mu]$ must be minimized in addition. The arbitrary gauge choice of a single instanton gauge field leads to a different value of $R_{ch}[A_\mu]$, although the instanton gauge field satisfies the condition (9) in any gauge [39]. For instance, in the singular gauge, which has a point singularity at the instanton center, the instanton configuration gives a finite value $R_{ch}[A^s_\mu]=4\pi^2\rho^2$ with ρ being the instanton size. On the other hand, in the nonsingular gauge, there appears the divergence as $R_{ch}[A^n_\mu]=2\int d^4x[\rho^2/(x^2+\rho^2)^2]\to\infty$. Therefore, it is necessary to consider the minimization of the functional $R_{ch}[A_\mu]$ for the MA gauge fixing.

Brower *et al.* consider the single instanton configuration in an ''intermediate'' gauge where the gauge field has the singularity at the closed loop with a radius R around its center [39]. This singularity leads a closed monopole loop of radius R around the instanton. The parameter R should be decided by minimizing the functional $R_{ch}[A_\mu]$. It is numerically shown that the monopole loop with radius R prefers to shrink to a point [39]. This fact is natural from the following consideration. There is no definite direction both in the single instanton configuration and in the MA gauge condition due to the 4-dimensional rotation invariance. Then, the normal vector of the monopole loop cannot be fixed and the loop ought to shrink to a point. However, the R dependence of $R_{ch}[A_\mu]$ is found to be extremely small. Therefore, some small perturbations as the presence of the finite volume cause a closed monopole loop with a nonzero radius R due to the fragile nature of the monopole point solution, which is first reported by Hart and Teper using the lattice simulation [35]. In the QCD vacuum, there are actually many instantons and anti-instantons, and here the appearance of monopole loops should be influenced by other instantons and anti-instantons. Therefore, we would like to investigate the monopole loops by using a more realistic multi-instanton system defined on the $\mathbf{R}^4$ space.

We first study the monopole clustering as a signal of monopole condensation in terms of instantons, which is motivated by these strong correlations between instantons and monopoles in the MA gauge. Second, we calculate the static quark potential in the multi-instanton system by using the Wilson loop in order to clarify the relation of instantons with color confinement.

IV. MULTI-INSTANTON MODEL

In this section, we would like to model the nonperturbative QCD vacuum in terms of instantons. The QCD vacuum possesses the gluon condensate [49], which relates the number of instantons and anti-instantons [5]. If the total action can be estimated as the sum of individual instanton actions, the gluon condensate is proportional to the instanton density as $\langle G^a_{\mu\nu}G^a_{\mu\nu}\rangle/32\pi^2 \simeq (N/V)$. The QCD sum rule provides the phenomenological value $\langle G^a_{\mu\nu}G^a_{\mu\nu}\rangle/32\pi^2 \simeq (200\ \mathrm{MeV})^4$, and hence the average instanton density becomes $(N/V)\simeq(1/\mathrm{fm})^4$ by the above assumption. The lattice QCD simulations suggest that the QCD vacuum is saturated with many instantons and anti-instantons. Hence, we model the QCD vacuum by the multi-instanton ensemble. First of all, we consider the partition function $\mathcal{Z}^1_{inst}$ of the single instanton as the basic ingredient of the multi-instanton theory. Using the collective coordinates, ρ, z_μ, O, the single-instanton partition function [5] is expressed as

$$\mathcal{Z}^1_{inst} = \int d^4 z_\mu \int d\rho \int dO f_0(\rho),$$

$$f_0(\rho) = \frac{C(N_c)}{\rho^5}\left[\frac{8\pi^2}{g^2(M)}\right]^{2N_c}(M\rho)^b \exp\left(-\frac{8\pi^2}{g^2(M)}\right), \tag{10}$$

with $b=\frac{11}{3}N_c$. Here, $f_0(\rho)$ is the single-instanton weight function in the one-loop approximation [50,51]. This weight function has a scale M corresponding to the scale invariance breaking by the trace anomaly in QCD. The bare coupling $g^2(M)$ is given at this scale M. The weight function $f_0(\rho)$ with $N_c \geqslant 2$ increases with the instanton size ρ, and the infrared divergence appears in $\mathcal{Z}^1_{inst}$ within the one-loop approximation.

We consider now the multi-instanton system. Based on the single-instanton partition function, the multi-instanton partition function is expressed as

$$\mathcal{Z} \propto \sum_{N_+ N_-} \frac{1}{N_+!}\frac{1}{N_-!}\prod_{n=1}^{N_+ + N_-}\int d^4 z_n \int d\rho_n \int dO_n f_0(\rho_n) \times \exp\{-U_{int}(z_n,\rho_n,O_n)\}, \tag{11}$$

where U_{int} denotes the interaction between instantons (anti-instantons) and depends generally on z_n, ρ_n, O_n. Here, we follow the standard method, where the interaction U_{int} is taken to depend only on the size ρ [52–54]. Therefore, we consider now $f(\rho)=f_0(\rho)\exp\{-U_{int}\}$ as the instanton size distribution. This interaction is found to be repulsive, which suppresses the appearance of large size instantons [52–54]. We regard the positions and the color orientations as random variables in our calculation.

For the small instanton, the perturbative scheme is valid and the interaction U_{int} can be neglected. Hence, the instanton size distribution $f(\rho)$ behaves as the single instanton weight $f_0(\rho)$,

$$f(\rho) \overset{\rho\to 0}{\to} \mathrm{const}\times\rho^{b-5}. \tag{12}$$

On the other hand, for the large instanton, the direct estimation of $f(\rho)$ is very complicated due to the nonperturbative properties. The analytical studies and the numerical lattice QCD calculations [55,56] suggest a strong suppression of the large size instanton as

$$f(\rho) \overset{\rho\to\infty}{\to} \mathrm{const}\times\rho^{-\nu}, \tag{13}$$

which is caused by the repulsive force in the infrared region. The ordinary instanton liquid model suggests $\nu=5$ [56].

To connect the two tendencies in Eqs. (12) and (13) smoothly, we take the size distribution as

$$f(\rho) = \frac{1}{\left(\frac{\rho}{\rho_1}\right)^{\nu} + \left(\frac{\rho_2}{\rho}\right)^{b-5}}, \tag{14}$$

where ρ_1 denotes the infrared size parameter and ρ_2 the ultraviolet size parameter. These two parameters are fixed by the average instanton size $\bar{\rho}\equiv\int_0^\infty d\rho\rho f(\rho)=0.4$ fm [57] and the normalization condition $\int_0^\infty d\rho f(\rho)=1$.

The above discussion leads to the use of the partition function

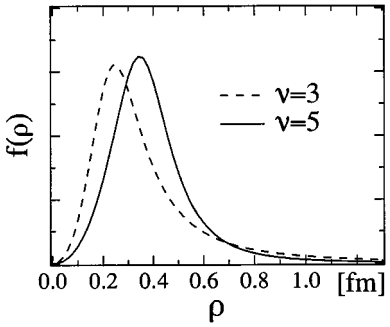

FIG. 1. The instanton size distribution $f(\rho)$ as a function of the instanton size ρ. The instanton size distribution for $\nu=5$ is denoted by solid curve and that for $\nu=3$ by dashed curve. In both cases, the average size $\bar{\rho}$ is kept to $\bar{\rho}=0.4$ fm.

$$\mathcal{Z}\propto\sum_{N_+N_-}\frac{1}{N_+!}\frac{1}{N_-!}\prod_{n=1}^{N_++N_-}\int d^4z_n\int_0^\infty d\rho_n\int dO_n \times\frac{1}{\left(\frac{\rho_n}{\rho_1}\right)^{\nu}+\left(\frac{\rho_2}{\rho_n}\right)^{b-5}}. \tag{15}$$

As for the gluon field A_μ of the multi-instanton system, we take the sum ansatz [58],

$$A_\mu(x)=\sum_k A^I_\mu(x;z_k,\rho_k,O_k)+\sum_k A^{\bar{I}}_\mu(x;z_k^-,\rho_k^-,O_k^-), \tag{16}$$

which is constructed by the instanton and anti-instanton solutions in the singular gauge. Using the variational treatment with this ansatz, Diakonov and Petrov have shown the appearance of the repulsive force between instanton and anti-instanton in the infrared region [58].

In actual calculations, we generate the ensemble of instantons and anti-instantons with random centers z_k on the 4-dimensional Euclidean continuum space. The color orientations O_k are taken randomly. The instanton sizes ρ_k are randomly chosen following the size distribution $f(\rho)$ in Eq. (14). In the simple sum ansatz, the interaction among these pseudoparticles is supposed to be included effectively in the instanton size distribution $f(\rho)$. The instanton size distribution for the cases of $\nu=5$ and 3 are shown in Fig. 1.

V. MONOPOLE CLUSTERING IN MULTI-INSTANTON SYSTEM

Based on the lattice gauge theory, we investigate monopole-loop distributions induced by instantons after the MA gauge fixing [43,44]. We introduce a lattice on the multi-instanton configuration and define the link variable $U_\mu(s)=\exp(iaA_\mu(s))$, where $A_\mu(s)$ is provided on each link from Eq. (16). In the actual calculation, we use the 32^4 lattice with the lattice spacing of $a=0.125$ fm.

First of all, let us discuss the boundary condition of the multi-instanton configuration. If instantons and anti-instantons are generated only in the finite volume $V=(32\times a)^4=(4.0\ \text{fm})^4$, the strength of the gluon field is insufficient near the border of the volume V. To avoid this border problem, we adopt the periodic boundary condition, which ensures adequate contributions also near the border. Here, instantons are assumed to appear with the periodic position, size and color orientation out of the finite volume V. A schematic view of this periodic condition of an instanton ensemble sliced into 2-dimensional plane is shown in Fig. 2. This means the consideration of the instantons in the 3^4 boxes in the 4-dimensional case: it is $3^2=9$ boxes in the 2-dimensional case as shown in Fig. 2. In actual calculation, we construct link variables by considering all the instantons in the neighboring boxes.

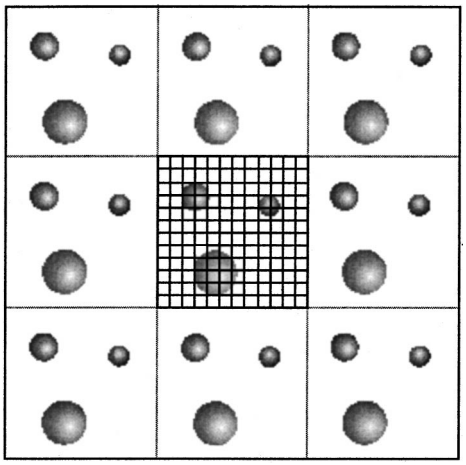

FIG. 2. A schematic demonstration of the periodic condition used for an instanton ensemble sliced into 2-dimensional plane. We introduce the lattice in the center of the instanton ensemble to calculate the link variables by considering all the instantons outside of this central box obtained with a periodic condition for the sizes, positions, and color orientations of instantons.

Now, we apply the MA gauge fixing [19] by maximizing

$$R_{able}=\sum_{\mu,s}\mathrm{tr}[U_\mu(s)\tau^3U_\mu^\dagger(s)\tau^3] =2\sum_{s,\mu}[1-2\{(U^1_\mu(s))^2+(U^2_\mu(s))^2\}], \tag{17}$$

with $U_\mu(s)=U^0_\mu(s)+i\tau^iU^i_\mu(s)$. The maximization of R corresponds to the lattice expression of the minimization condition of $R_{ch}[A_\mu]$ in Eq. (4). In the MA gauge, the SU(2) link variable $U_\mu(s)$ is decomposed as

$$U_\mu(s)=M_\mu(s)u_\mu(s)=\begin{pmatrix}\sqrt{1-|c_\mu(s)|^2} & -c^*_\mu(s)\\ c_\mu(s) & \sqrt{1-|c_\mu(s)|^2}\end{pmatrix}\times\begin{pmatrix}e^{i\theta_\mu(s)} & 0\\ 0 & e^{-i\theta_\mu(s)}\end{pmatrix}, \tag{18}$$

where the Abelian angle variable $\theta_\mu(s)$ and the non-Abelian variable $c_\mu(s)$ are defined in terms of $U_\mu(s)$ as

$$\tan\theta_\mu(s)=\frac{U^3_\mu(s)}{U^0_\mu(s)},\ c_\mu(s)e^{i\theta_\mu(s)}=[-U^2_\mu(s)+iU^1_\mu(s)]. \tag{19}$$

It is obvious from the expression of Eq. (17) that the off-diagonal parts $U^1_\mu(s)$ and $U^2_\mu(s)$ of gluon fields are minimized by the MA gauge transformation. Therefore, full SU(2) link variables would be approximated as U(1) link variables, $U_\mu(s)\simeq u_\mu(s)$, in the MA gauge.

Monopole currents can be defined by using $u_\mu(s)$ following DeGrand and Toussaint [59]. Using a forward derivative $\partial_\mu f(s)\equiv f(s+\hat{\mu})-f(s)$ with unit vector $\hat{\mu}$, the 2-form of the lattice formulation, $\theta_{\mu\nu}(s)\equiv\partial_\mu\theta_\nu(s)-\partial_\nu\theta_\mu(s)$, is decomposed as

$$\theta_{\mu\nu}(s)=\overline{\theta}_{\mu\nu}(s)+2\pi n_{\mu\nu}(s), \tag{20}$$

with $\overline{\theta}_{\mu\nu}(s)\equiv \mathrm{mod}_{2\pi}\theta_{\mu\nu}\in(-\pi,\pi]$ and $n_{\mu\nu}(s)\in\mathbf{Z}$. Here, $\overline{\theta}_{\mu\nu}(s)$ and $2\pi n_{\mu\nu}(s)$ correspond to the regular field strength and the singular Dirac string part, respectively. Since the Abelian Bianchi identity is broken, the monopole current $k_\mu(^*s)$ can be defined on the dual link $(^*s,\mu)$ as

$$k_\mu(^*s)\equiv\frac{1}{4\pi}\varepsilon_{\mu\nu\alpha\beta}\partial_\nu\overline{\theta}_{\alpha\beta}(s+\hat{\mu})=-\partial_\nu\tilde{n}_{\mu\nu}(^*s), \tag{21}$$

where $\tilde{n}_{\mu\nu}(^*s)\equiv\frac{1}{2}\varepsilon_{\mu\nu\alpha\beta}n_{\alpha\beta}(s+\hat{\mu})$. The obvious current-conservation law $\partial'_\mu k_\mu(^*s)=0$ leads to the closed monopole loop in the 4-dimensional space. Here, ∂'_μ denotes a backward derivative.

Since we are interested in the infrared behavior of monopoles in multi-instanton configurations, it is useful to execute a ''block-spin'' transformation on the dual lattice with the scale factor $\mathcal{N}$. The ''block-spin'' transformation removes small monopole loops as numerical noises and keeps its global structure. Here, the $\mathcal{N}^3$ extended monopole is defined as

$$n^{\mathcal{N}}_{\alpha\beta}(s)\equiv\sum_{i,j=0}^{\mathcal{N}-1}n_{\alpha\beta}(\mathcal{N}s+i\hat{\alpha}+j\hat{\beta}) \tag{22}$$

on a sublattice with the spacing of $b=\mathcal{N}a$ [60]. Then, the extended monopole current is defined as $k^{\mathcal{N}}_\mu(^*s)=-\frac{1}{2}\varepsilon_{\mu\nu\alpha\beta}\partial_\nu n^{\mathcal{N}}_{\alpha\beta}(s+\hat{\mu})$.

We start with a very dilute instanton system in order to clarify a local correlation between instantons and monopoles in the MA gauge. We take a density $(N/V)\ll(0.5/\mathrm{fm})^4=(100\,\mathrm{MeV})^4$, where instantons are separated completely from each other. From the analytical consideration, one may expect that a monopole loop prefers to shrink to a instanton center. However, we observe on the lattice that each finite-size monopole loop is localized around each instanton center as shown in Fig. 3(a). Such a small monopole but finite-size loop is caused by finite lattice spacing and the boundary effect, which is numerically washed out by several numbers of ''block-spin'' transformation.

In the actual QCD vacuum, instantons saturate the 4-dimensional space and stay close to each other with a instanton density of $(N/V)=(1/\mathrm{fm})^4$ [6]. Therefore, we consider three instanton number-density cases, $(N/V)^{1/4}=0.75$, 1.00 and 1.25 fm^{-1}, and investigate the behaviors of monopole loops. Figure 4(a) shows the histograms of unblocked monopole loops. The histograms of blocked configurations are shown in Figs. 4(b)–4(d), which corresponds to the extended monopoles on the sublattice with $b=2a$, $b=4a$ and $b=8a$, respectively.

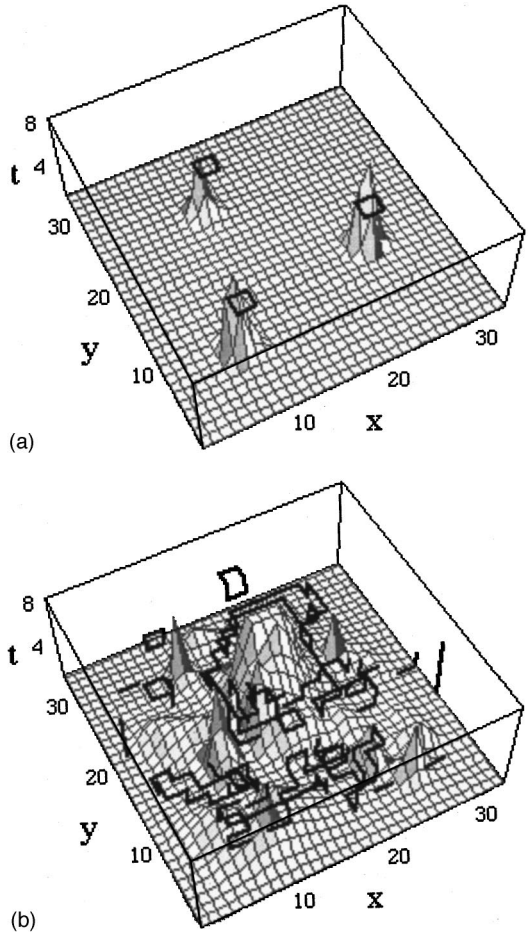

FIG. 3. The local correlation between instantons and monopoles for a dilute instanton system (a), and for a dense instanton system (b). The thick lines denote monopole currents which appear at some time t. The bottom surface corresponds to the action density of instantons $s(x,y)$ at a certain time slice. Here, we show monopole currents which are transformed by one ''block-spin'' on the $32^2\times8^2$ lattice with $a=0.125$ fm.

At the low instanton density where each instanton is isolated, the monopole loop induced by the instanton prefers to be localized around each instanton center as shown in Fig. 3(a). Thus, there appear only relatively short monopole loops. This situation provides a peak at zero monopole-loop length in the histogram as shown in Fig. 4(d-i). As the instanton density increases, some monopole trajectories tend to hop from one instanton to another nearby instanton as shown in Fig. 3(b), and there appear long monopole loops. Here, a clustering of long monopole loops appears and grows gradually to be separated from the small monopole-loop part in the histogram. Furthermore, the ''block-spin'' transforma-

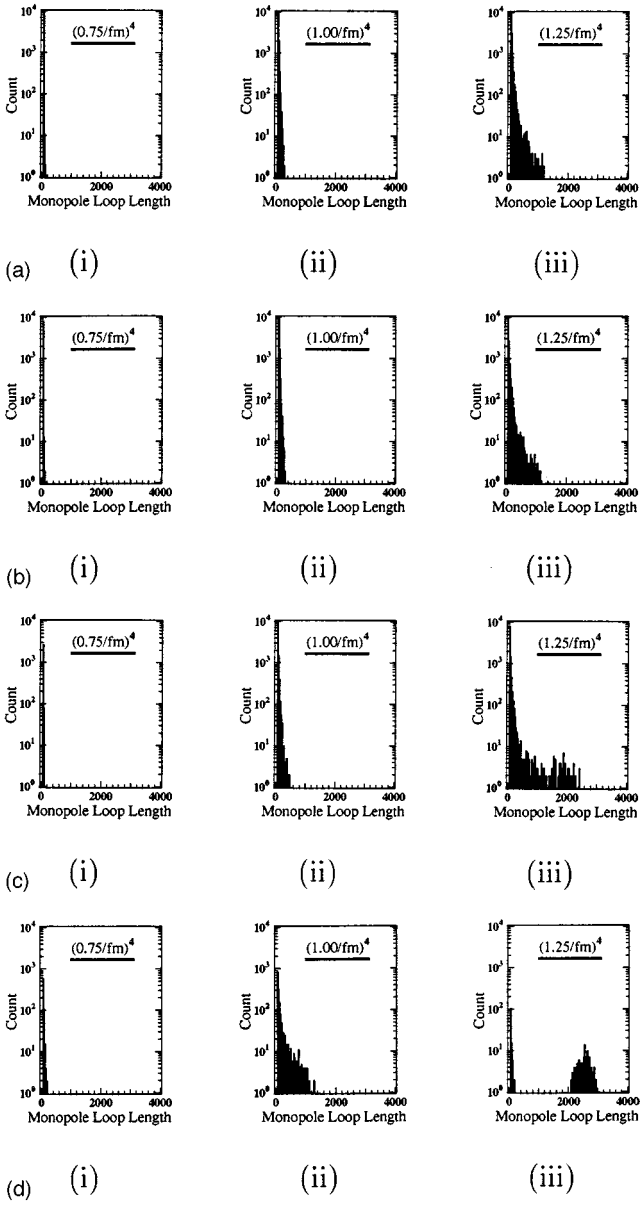

FIG. 4. The histograms of monopole-loop length with various densities $(N/V)^{1/4}=0.75$, 1.0 and 1.25 fm^{-1}, after the various ''block-spin'' transformations in the $\nu=5$ case. (a) denotes the results of no ''block-spin'' transformation. (b), (c) and (d) denote the results after one, two and three ''block-spin'' transformations, respectively.

tion is available to clarify monopole loop behaviors at the large scale by comparing Figs. 4(a-iii), (b-iii), (c-iii) and (d-iii). Because this procedure removes small-size monopole loops and combine several long monopole-loops into one longer loop. At a high instanton density, there appears one very long and highly complicated monopole loop in each gauge configuration as shown in Fig. 4(d-iii). Such an appearance of the monopole clustering over the entire physical volume can be interpreted as the Kosterlitz-Thouless-type phase transition [61,62].

In addition, we discuss the case of the instanton size distribution $\nu=3$ with the average size $\bar{\rho}=0.4$ fm as shown in Fig. 1. Diakonov pointed out that if the instanton size distribution falls off as $f(\rho)\sim 1/\rho^3$ in the infrared region, one gets a linear confinement potential [55], which is based on the formula for the interquark potential in Ref. [63]. Since instantons tend to have large overlapping from each other for the $\nu=3$ case, the simple treatment with the sum ansatz, which is based on the assumption of the statistical independence, may not be applicable for the construction of the multi-instanton system. However, the infrared behavior of the instanton size distribution is interesting for the confinement properties in the long-range region. Therefore, we demonstrate also the $\nu=3$ case. The histograms of the $\nu=3$ case are qualitatively similar to the corresponding histograms of the $\nu=5$ case, although there is a quantitative difference between these two cases.

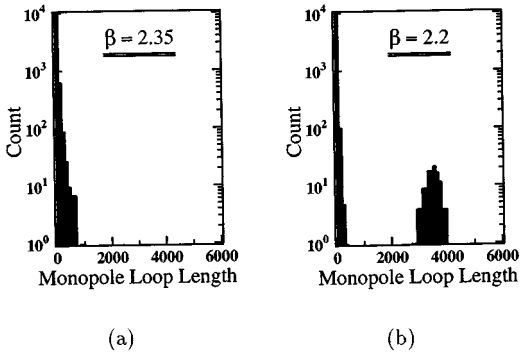

FIG. 5. The histograms of monopole-loop length in unit of the lattice spacing a at high temperature (a), and at low temperature (b) in finite temperature $SU(2)$ lattice QCD.

Lattice QCD simulations at finite temperature suggest that the instanton density is largely reduced as the temperature increases. Now, we compare the histograms of the monopole loop length in the multi-instanton system with those of the SU(2) lattice QCD with $16^3\times 4$ at different temperatures ($\beta=2.2$ and 2.35) in Fig. 5 [41]. The monopole-loop distribution at high instanton-density case as shown in Fig. 4(d-iii) resembles with the result of the confinement phase ($\beta=2.2$) in Fig. 5(b), where many instantons and anti-instantons saturate with the instanton density $(N/V)\simeq(1/\text{fm})^4$. On the other hand, the dilute instanton system as shown in Fig. 4(d-i) is similar to the result in the deconfinement phase in Fig. 5(a) obtained by the lattice QCD ($\beta=2.35$), where long monopole loops disappear. This resemblance seems to indicate that the instanton plays a relevant role on the promotion of monopole loops in the confinement phase.

VI. COLOR CONFINEMENT IN MULTI-INSTANTON SYSTEM

In the previous section, we have discussed that a high-density instanton system provides highly complicated monopole loops. We shall further work out the confining property in the multi-instanton system without referring to monopole configurations in the MA gauge [64]. For the investigation of confinement properties, it is reasonable to consider the Wilson loop with a contour C, which is defined as

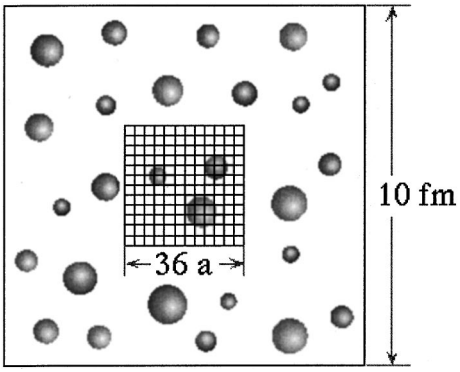

FIG. 6. A random instanton configuration without the periodic condition for sizes, positions and color orientations of instantons sliced into 2-dimensional plane. We introduce the lattice in the center of the random instanton ensemble. a denotes the lattice unit and 36 corresponds to the number of lattice point in each time-space direction.

$$W[C] \equiv \mathrm{tr}\, \mathrm{P} \exp\left[i \oint_C A_\mu dx_\mu \right] = \mathrm{tr} \prod_C U_\mu(s). \qquad (23)$$

If the contour C is a rectangle of the dimension T by R, the Wilson loop is related to the static quark potential [65] as

$$V(R) = -\lim_{T\to\infty} \{\ln W(R,T)/T\}. \qquad (24)$$

To extract the potential without the contamination of excited states, the time T has to be large enough compared to the distance R between quark and anti-quark, $T \gg R$ [66]. Hence, it is desired to take a large enough T in the calculation of $W[C]$. In the periodic boundary conditions, the time distance is limited as a half of $N_t \times a$, where N_t is the number of lattice in the time direction and a is the lattice unit. Therefore, we introduce the 36^4 lattice in the center of a 4-dimensional instanton configurations without the periodic condition for the sizes, positions and color orientations of instantons. Here, the large Wilson loop can be calculated as $T \simeq 36 \times a$ because of the nonperiodic boundary. A schematic view of this condition sliced into 2-dimensional plane is shown in Fig. 6.

In our actual calculation, we consider the instanton configuration with the entire volume of $V = (10\,\mathrm{fm})^4$. We have to fix now the lattice-spacing a. For instance, the instanton density $(N/V) = (1/\mathrm{fm})^4$ corresponds the instanton number $N = N_+ + N_- = 10^4$ in the volume $(10\,\mathrm{fm})^4$. Since the gluon gauge field is constructed from the summation of instantons and anti-instantons as $A_\mu(s) = \Sigma_{N_+,N_-}(A^I_\mu + A^{\bar{I}}_\mu)$, a fine lattice-spacing is necessary to justify the continuity of the link variables $U(s) = \exp[iaA_\mu(s)]$ in above situation. Therefore, we actually take a fine lattice spacing of $a = 0.05\,\mathrm{fm}$ considering the continuity, $aA_\mu(s) \ll 1$.

Recent lattice QCD simulations provide us the average instanton size $\bar{\rho}$ and the instanton density (N/V). The instanton properties are extracted from the smoothed QCD vacuum by using several cooling methods. DeGrand *et al.* investigate a smoothing procedure based on the renormalization group equation [13]. In this SU(2) lattice calculation, they find the average size of instantons about $\bar{\rho} = 0.2$ fm, which is too small a value than that of usual instanton liquid model, at a density of about $(N/V) = 2\ \mathrm{fm}^{-4}$. On the other hand, de Forcrand *et al.* use a cooling algorithm based on the improved action with scale invariant instanton solution and provide that the instanton size distribution is peaked around 0.43 fm. [12]. These two cooling methods provide different values about the average instanton size. As for the instanton size distribution, there are much effort to extract a size distribution from the lattice configurations by various smoothing methods [11–14]. However, there is no consensus on the size distribution either. In our calculation, we take the instanton density as $(N/V) = (1/\mathrm{fm})^4$ and the average instanton size $\bar{\rho} = 0.4$ fm. These parameters are used in the discussion of chiral symmetry breaking [67] and give us the monopole length distribution in the range of those obtained by QCD simulation as shown in the previous section [44]. For simplicity, we consider the typical case where the instanton number is equal to the anti-instanton one, $N_I = N_{\bar{I}} = N/2$.

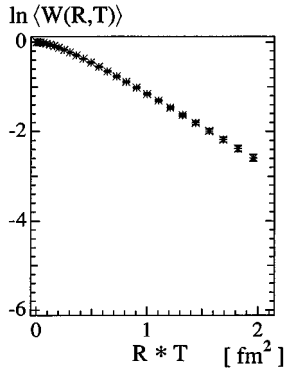

FIG. 7. The ensemble average of the Wilson loop in the multi-instanton system with the infrared instanton size distribution of $\nu = 5$ as a function of the area $R \times T$. The instanton density is $(N/V)^{1/4} = 1\ \mathrm{fm}^{-1}$ and the average size is $\bar{\rho} = 0.4$ fm.

Using the large 36^4 lattice without periodic boundary condition, we can make as many as 10^4 measurements of Wilson loops for each instanton configuration. Actually, we estimate the expectation value of Wilson loops from about 5×10^6 measurements of Wilson loops on 500 completely independent configurations. Figure 7 shows the Wilson loop for the case of $\nu = 5$. The Wilson loop seems to decay as $\langle W(R,T) \rangle \propto \exp[-\sigma RT]$, which indicates the existence of a linear confining potential. As shown in Fig. 8, the static quark potential $V(R)$ is proportional to the interquark distance R up to the intermediate region $R \simeq 1.2\,\mathrm{fm}$ $(< T)$. Here, we have checked that the static potential at $R \leqslant 1.2$ fm does not depend on T $(\gg R)$ within errors. We speculate that instantons would be relevant degrees of freedom for the linear potential between a quark and anti-quark pair in the physically interesting region.

The area low behavior of the Wilson loop means that the errors of this value grow as the area RT increases, since the Wilson loop decreases exponentially with RT. The static quark potential is not yet demonstrated at longer distance region as $R > 1.2$ fm, where it is necessary to calculate

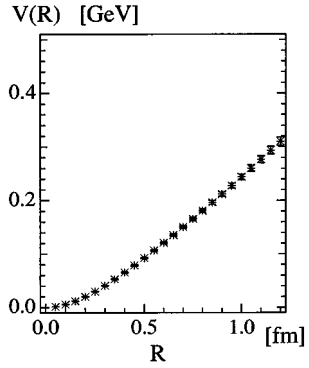

FIG. 8. The static potential in the multi-instanton system as a function of the distance R extracted from the Wilson loop with $T=1.8$ fm of Fig. 7.

larger Wilson loops with $T \gg 2.0$ fm. To this end, we need a huge number of independent measurements and perform the smearing procedure to reduce the statistical error because of the small value of Wilson loops $\langle W(R,T)\rangle \propto \exp[-\sigma RT]$.

Finally, we discuss the relation between the strength of color confinement and the instanton density. In order to extract the string tension, we measure the Creutz ratio

$$\chi(R,T) \equiv \frac{\langle W(R,T)\rangle\langle W(R-1,T-1)\rangle}{\langle W(R,T-1)\rangle\langle W(R-1,T)\rangle} \tag{25}$$

from the SU(2) Wilson loop. If the logarithm of the Wilson loop can be approximated as $-\ln\langle W(R,T)\rangle = \sigma RT + m(R+T) + \text{const}$, the Creutz ratio gives the exponent of the string tension, $\chi = \exp(-\sigma_{lat})$. The dimensionless lattice string tension σ_{lat} provides the physical string tension σ_{phys} with the lattice-spacing a as $\sigma_{phys} = \sigma_{lat}/a^2$.

We estimate the string tension around $R \simeq 0.8$ fm for each instanton density, $(N/V)^{1/4} = 0.50$, 0.75 and 1.0 fm^{-1}. As shown in Fig. 9, the string tension depends directly on the instanton density, and grows drastically as the instanton density increases. At a density of $(N/V) = (1/\text{fm})^4$ with $\nu = 5$, the string tension comes out to be about $\sigma \simeq 0.4$ GeV/fm, which corresponds to about a half of the physical string tension $\sigma_{exp} \simeq 0.89$ GeV/fm.

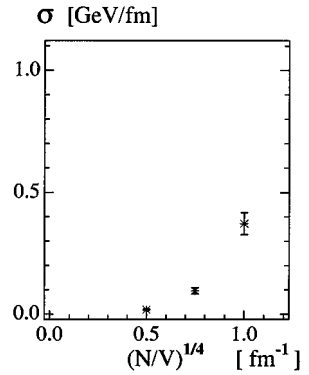

FIG. 9. The string tension σ as a function of the instanton density $(N/V)^{1/4}$ with the infrared instanton size distribution $\nu = 5$.

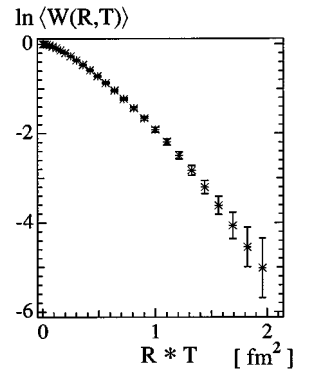

FIG. 10. The ensemble average of the Wilson loop in the multi-instanton system with the infrared instanton size distribution $\nu = 3$ as a function of the area $R \times T$. The instanton density and the average size are kept the same as the case of $\nu = 5$.

In addition, we demonstrate the $\nu = 3$ case. As shown in Fig. 10 and Fig. 11, the Wilson loop seems to obey the area low and there appear a linear potential at $R \leqslant 1.2$ fm, which are qualitatively similar to the $\nu = 5$ case. Figure 12 shows that the string tension of the $\nu = 3$ case is larger than that of the $\nu = 5$ case at the same density, which is caused by the large overlapping of instantons and anti-instantons in the $\nu = 3$ case. Rigorously speaking, for $\nu = 3$ it may not be suitable to adopt the simple sum ansatz, which is based on the statistical independence of the instanton ensemble. Therefore, one needs to construct a new formulation, which is workable also for the highly overlapping instanton system as the $\nu = 3$ case.

Finally, we would like to discuss the difference of the present results with the previous works. In our previous calculation [64], we fixed the peak of the instanton size distribution as $\rho_{peak} = 0.4$ fm, which corresponds to the average instanton size of $\bar{\rho} \simeq 0.45$ fm. We extracted then the static potential using smaller Wilson loops. Since the string tension strongly depends also on the average instanton size $\bar{\rho}$, we obtained a larger value for the string tension [64] than that of the present calculation. Recently, Brower *et al.* report that the slope of the heavy quark potential is about 0.1 GeV/fm at the average instanton size $\bar{\rho} = 1/3$ fm and the density

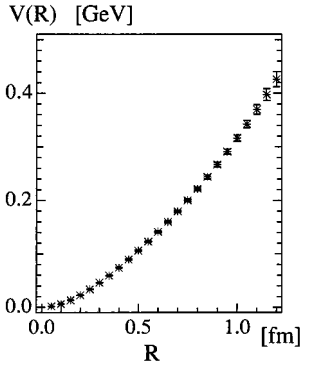

FIG. 11. The static potential in the multi-instanton system as a function of the distance R extracted from the Wilson loop of Fig. 10.

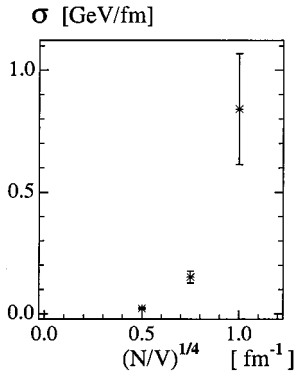

FIG. 12. The string tension σ as a function of the instanton density $(N/V)^{1/4}$ with the infrared instanton size distribution $\nu=3$.

$(N/V)=(1/\mathrm{fm})^4$ [68]. The main reason of the discrepancy is the different choice of the average instanton size $\bar{\rho}$. In addition, they use larger Wilson loops with T above 3 fm. The large Wilson loop justifies the extraction of the string tension. In this sense, they should obtain a better value for the string tension at long distance [68]. However, in their calculation, the perpendicular 2-dimensional directions $(x-y)$ to the plane $(z-t)$ of Wilson loops are limited to be much narrower than the size of the Wilson loop, although the other directions are very wide for the calculation of large Wilson loops. Our preliminary study of the contributions of instantons away from the plane of the Wilson loop in the $x-y$ plane indicates appreciable contributions to such a large Wilson loop. Hence, it would be necessary to consider a large volume even in the $x-y$ direction for the large Wilson loop, which is outside of the scope of this work.

VII. SUMMARY AND CONCLUSION

We have studied color confinement and nonperturbative quantities of the QCD vacuum using the multi-instanton configuration. We have made the present study by being motivated by the presence of a strong correlation between instantons and monopoles after the Abelian gauge fixing in pure SU(2) gauge theory. In our calculation, the multi-instanton system is constructed by assuming the suppression of the large size instanton as $f(\rho)\sim\rho^{-5}$ due to the infrared repulsive interaction between instantons.

First, we have investigated the monopole-loop distribution in the multi-instanton system by using the maximally Abelian gauge. Here, we have executed the ''block-spin'' transformation in order to extract the infrared properties of monopole loops. The dilute-instanton system produces small monopole loops localized around each isolated instanton. If instantons are well separated each other, monopole loops disappear in the continuum limit $a\to 0$. However, as the instanton density becomes higher, several small monopole loops combine into one longer loop. At a high instanton density, there appears a highly complicated monopole loop covering the entire physical volume. The appearance of long monopole loops of this system resembles that of the low-temperature lattice QCD where color confinement is realized through monopole condensation [48]. Our results indicate that instantons play an essential role on the promotion of a global network of monopoles.

We have found that the high instanton density provides a highly complicated and long monopole loop. This seems to indicate that instantons are responsible also for confinement. Therefore, we have calculated the Wilson loop in the multi-instanton system without the Abelian gauge fixing. Here, we take the instanton density of $(N/V)=(1/\mathrm{fm})^4$ and the average instanton size of $\bar{\rho}=0.4$ fm. We have found that the instanton ensemble gives an area law behavior of the Wilson loop and the static quark potential is approximately proportional to the interquark distance, $V(R)\simeq\sigma R$, up to $R\simeq 1.2$ fm. In this situation, the string tension has been evaluated as $\sigma\simeq 0.4$ GeV/fm, which corresponds to about a half of the physical string tension $\sigma_{exp}\simeq 0.89$ GeV/fm. Furthermore, we have discussed the dependence of the string tension on the instanton density. The string tension tends to decrease monotonously as the instanton density becomes smaller. Such a tendency is consistent with the disappearance of long monopole loop as the instanton number decreases. At the high temperature QCD vacuum where the string tension is zero, instantons and anti-instantons almost disappear and also the long monopole loops do. From this close relation between the monopole clustering and the instanton density, we speculate that instantons would be relevant degrees of freedom for the linear potential between quark and antiquark in the physically interesting region.

In the multi-instanton system, the string tension depends directly on both the instanton density and the average instanton size. Therefore, one has to fix these parameters from the original QCD vacuum. To this end, for instance, the improved cooling [12] and the inverse-blocking [13] are very interesting scheme for the extraction of topological quantities like instantons. Finally, it is necessary to simulate the static quark potential at longer distance ($R\gg 1.2$ fm) using larger Wilson loops and enormous configurations in order to clarify the confinement properties up to very long distance. However, the calculation of such a large Wilson loop would be facing the limit of the present computation power.

ACKNOWLEDGMENTS

We would like to thank Dr. S. Sasaki for his useful comments and discussions. M.F. would like to thank Dr. A. Tanaka for his continuous encouragement. One of the authors (H.S.) is supported in part by Grant for Scientific Research (No.09640359) from the Ministry of Education, Science and Culture, Japan. One of the authors (M.F.) is supported by Japan Society for the Promotion of Science for Young Scientists. We have performed all numerical simulations with NEC SX4 of Osaka University.

[1] A. Belavin, A. Polyakov, A. Shvarts, and Yu. Tryupkin, Phys. Lett. **59B**, 85 (1975).
[2] R. Rajaraman, *Solitons and Instanton* (North-Holland, Amsterdam, 1982), p. 1.
[3] G. 't Hooft, Phys. Rev. Lett. **37**, 8 (1976); Phys. Rev. D **14**, 3432 (1976).
[4] E. Shuryak and J. Verbaarschot, Nucl. Phys. **B341**, 1 (1990).
[5] D. Diakonov, hep-ph/9602375.
[6] T. Schäfer and E. Shuryak, Rev. Mod. Phys. **70**, 323 (1998).
[7] A. Polyakov, Nucl. Phys. **B120**, 429 (1977).
[8] M. Teper, Phys. Lett. **162B**, 357 (1985).
[9] M. Polikarpov and A. Veselov, Nucl. Phys. **B297**, 34 (1988).
[10] M. Campostrini, A. Di Giacomo, H. Panagopoulos, and E. Vicari, Nucl. Phys. **B329**, 683 (1990).
[11] C. Michael and P. Spencer, Phys. Rev. D **52**, 4691 (1995).
[12] P. de Forcrand, M. Perez, and I. Stamatescu, Nucl. Phys. **B499**, 409 (1997).
[13] T. DeGrand, A. Hasenfrantz, and T. Kovacs, Nucl. Phys. **B520**, 301 (1998).
[14] J. Negele, hep-lat/9810053.
[15] G. 't Hooft, Nucl. Phys. **B190**, 455 (1981).
[16] Y. Nambu, Phys. Rev. D **10**, 4262 (1974).
[17] G. 't Hooft, *High Energy Physics* (Editorice Compositori, Bologna, 1975.).
[18] S. Mandelstam, Phys. Rep., Phys. Lett. **23C**, 245 (1976).
[19] A. Kronfeld, G. Schierholz, and U.-J. Wiese, Nucl. Phys. **B293**, 461 (1987).
[20] A. Kronfeld, M. Laursen, G. Schierholz, and U.-J. Wiese, Phys. Lett. B **198B**, 516 (1987).
[21] F. Brandstater, U.-J. Wiese, and G. Schierholz, Phys. Lett. B **272**, 319 (1991).
[22] S. Hioki, S. Kitahara, S. Kiura, Y. Matsubara, O. Miyamura, S. Ohno, and T. Suzuki, Phys. Lett. B **272**, 326 (1991).
[23] S. Kitahara, Y. Matsubara, and T. Suzuki, Prog. Theor. Phys. **93**, 1 (1995).
[24] O. Miyamura, Phys. Lett. B **353**, 9 (1995); Nucl. Phys. B (Proc. Suppl.) **42**, 538 (1995).
[25] R. Woloshyn, Phys. Rev. D **51**, 6411 (1995).
[26] H. Suganuma, S. Sasaki, and H. Toki, Nucl. Phys. **B435**, 207 (1995).
[27] S. Sasaki, H. Suganuma, and H. Toki, Prog. Theor. Phys. **94**, 733 (1995).
[28] S. Sasaki, H. Suganuma, and H. Toki, Phys. Lett. B **387**, 145 (1996).
[29] H. Suganuma, K. Itakura, H. Toki, and O. Miyamura, *Nonperturbative Approaches to QCD* (PNPI, Gatchina, 1995), p. 224.
[30] H. Suganuma, H. Ichie, S. Sasaki, and H. Toki, *Color Confinement and Hadrons* (World Scientific, Singapore, 1995), p. 65.
[31] O. Miyamaura and S. Origuchi, *Color Confinement and Hadrons* (World Scientific, Singapore, 1995), p. 235.
[32] S. Thurner, H. Markum, and W. Sakuler, *Color Confinement and Hadrons* (World Scientific, Singapore, 1995), p. 77.
[33] M. Chernodub and F. Gubarev, Pis'ma Zh. Eksp. Teor. Fiz. **62**, 104 (1995) [JETP Lett. **62**, 100 (1995)].
[34] H. Suganuma, A. Tanaka, S. Sasaki, and O. Miyamura, Nucl. Phys. B (Proc. Suppl.) **47**, 302 (1996).
[35] A. Hart and M. Teper, Phys. Lett. B **371**, 261 (1996).
[36] H. Markum, W. Sakuler, and S. Thurner, Nucl. Phys. B (Proc. Suppl.) **254**, 47 (1996).
[37] S. Thurner, M. Feurstein, H. Markum, and W. Sakuler, Phys. Rev. D **54**, 3457 (1996).
[38] V. Bornyakov and G. Schierholz, Phys. Lett. B **384**, 190 (1996).
[39] R. Brower, K. Originos, and C. Tan, Phys. Rev. D **55**, 6313 (1997;).
[40] M. Polikarpov, Nucl. Phys. B (Proc. Suppl.) **53**, 134 (1997).
[41] H. Suganuma, S. Sasaki, H. Ichie, H. Toki, and A. Araki, *Frontier '96* (World Scientific, Singapore, 1997); p. 177; H. Suganuma, S. Sasaki, H. Ichie, F. Araki, and O. Miyamura, Nucl. Phys. B (Proc. Suppl.) **53**, 528 (1997).
[42] S. Thurner, M. Feurstein, and H. Markum, Phys. Rev. D **56**, 4039 (1997).
[43] M. Fukushima, A. Tanaka, S. Sasaki, H. Suganuma, H. Toki, and D. Diakonov, Nucl. Phys. B (Proc. Suppl.) **53**, 494 (1997).
[44] M. Fukushima, S. Sasaki, H. Suganuma, A. Tanaka, H. Toki, and D. Diakonov, Phys. Lett. B **399**, 141 (1997).
[45] S. Sasaki and O. Miyamura, Phys. Lett. B **443**, 331 (1998).
[46] S. Sasaki and O. Miyamura, Phys. Rev. D **59**, 094507 (1999).
[47] E. Ilgenfritz, H. Markum, M. Mueller-Preussker, and S. Thurner, Phys. Rev. D **58**, 094502 (1998).
[48] H. Suganuma, H. Ichie, A. Tanaka, and K. Amemiya, Prog. Theor. Phys. Suppl. **131**, 559 (1998).
[49] M. Shifman, A. Vainshtein, and V. Zakharov, Nucl. Phys. **B147**, 385 (1979).
[50] G. 't Hooft, Phys. Rev. Lett. **37**, 8 (1976).
[51] C. Bernard, Phys. Rev. D **19**, 3013 (1979).
[52] D. Diakonov and V. Petrov, Phys. Rev. D **50**, 266 (1994).
[53] E. Shuryak and J. Verbaarschot, Phys. Rev. D **52**, 295 (1995).
[54] E. Shuryak, *The QCD Vacuum, Hadron and The Superdense Matter* (World Scientific, Singapore, 1988), p. 1.
[55] D. Diakonov and V. Petrov, *Non-Perturbative Approaches to QCD* (Ref. [29]), p. 239.
[56] E. Shuryak, Phys. Rev. D **52**, 5370 (1995).
[57] E. Shuryak, Nucl. Phys. **B203**, 93 (1982); **B203**, 116 (1982).
[58] D. Diakonov and V. Petrov, Nucl. Phys. **B245**, 259 (1984).
[59] T. DeGrand and D. Toussaint, Phys. Rev. D **22**, 2478 (1980).
[60] T. L. Ivanenko, A. V. Pochinskii, and N. I. Polikarpov, Phys. Lett. B **252**, 631 (1990).
[61] J. M. Kosterlitz, and D. J. Thouless, J. Phys. C **6**, 1181 (1973).
[62] H. Ichie, H. Suganuma, and A. Tanaka, Nucl. Phys. **A629**, 82c (1998).
[63] D. Diakonov and V. Petrov, Phys. Lett. B **226**, 372 (1989).
[64] M. Fukushima, H. Suganuma, A. Tanaka, H. Toki, and S. Sasaki, Nucl. Phys. B (Proc. Suppl.) **63A-C**, 513 (1998).
[65] H. Rothe, *Lattice Gauge Theory* (World Scientific, Singapore, 1992), p. 1.
[66] D. Diakonov and V. Petrov, hep-lat/9810037.
[67] D. Diakonov and V. Petrov, Phys. Lett. **147B**, 351 (1984).
[68] R. Brower, D. Chen, J. Negele, and E. Shuryak, Nucl. Phys. B (Proc. Suppl.) **73**, 512 (1999).